S1 Derivation of ΔVOC_{min}

An expression for ΔVOC_{min}, the minimum amount of VOC reacted for SOA formation, can be obtained by rearranging Eq. (2) and (3),

$$\frac{1}{\Delta VOC} = \frac{\sum_i \alpha_i \xi_i}{C_{OA}} = \frac{\sum_i \alpha_i \left(1+\frac{C_i^*}{C_{OA}}\right)^{-1}}{C_{OA}}$$

$$\frac{1}{\Delta VOC} = \frac{C_{OA}}{C_{OA}} \sum_i \frac{\alpha_i}{C_i^* + C_{OA}}$$

$$\frac{1}{\Delta VOC} = \sum_i \frac{\alpha_i}{C_i^* + C_{OA}}$$

$$\frac{1}{\Delta VOC_{\min}} = \sum_i \frac{\alpha_i}{C_i^*} \qquad (C_{OA} = 0)$$

The same expression can also be obtained via L'Hôpitals' rule,

$$\lim_{C_{OA}\to 0} \frac{1}{\Delta VOC} = \lim_{C_{OA}\to 0} \frac{C_{OA}}{C_{OA}} \left[\frac{\alpha_1}{C_1^* + C_{OA}} \dots \frac{\alpha_n}{C_n^* + C_{OA}}\right]$$

$$\lim_{C_{OA}\to 0} \frac{1}{\Delta VOC} = \lim_{C_{OA}\to 0} \frac{\frac{d}{dC_{OA}}\left[C_{OA} \sum_i \left(\frac{\alpha_i}{C_i^*} \prod_j C_j^*\right) + C_{OA}{}^{0}(\dots) + C_{OA}{}^{M\geq 2}(\dots)\right]}{\frac{d}{dC_{OA}}\left[C_{OA} \prod_j C_j^* + C_{OA}{}^{0}(\dots) + C_{OA}{}^{M\geq 2}(\dots)\right]}$$

$$\lim_{C_{OA}\to 0} \frac{1}{\Delta VOC} = \lim_{C_{OA}\to 0} \left[\frac{\prod_j C_j^* \sum_i \frac{\alpha_i}{C_i^*}}{\prod_j C_j^*}\right] = \sum_i \frac{\alpha_i}{C_i^*}$$

Where the terms involving C_{OA}^{0} become 0 and the terms involving $C_{OA}^{M\geq 2}$ are much smaller than terms involving $C_{OA}^{M\leq 1}$, and could therefore be neglected.

S2 SOA oxidation state parameterization

From f_{44}, O:C, H:C, and $\mathrm{OS_c}$ can be estimated as described in the literature (Canagaratna et al., 2015; Donahue et al., 2012; Heald et al., 2010; Kroll et al., 2011)

$$O:C = 0.079 + 4.31 \times f_{44}\ , \tag{S-1}$$

$$H:C = 2 - O:C\ , \tag{S-2}$$

$$\overline{OS}_C \cong 3 \times O:C - 2\ , \tag{S-3}$$

$$\overline{OS}_C \cong 12.93 \times f_{44} - 1.842\ , \tag{S-4}$$

To estimate the effect of vapor wall loss, UV lights were turned off early during Exp. A5. As shown in Fig S1, SOA oxidation states (f_{44} and f_{43}) were stable in the absence of UV, indicating that dark reactions, if present, were insignificant. Some wall-loss-corrected SOA concentration decrease was observed in the dark, likely due to loss of organic vapor to the clean chamber wall. The magnitude of vapor wall loss was minor compared to oxidative fragmentation loss, as shown in Fig. S1 during the second photo-oxidation period.

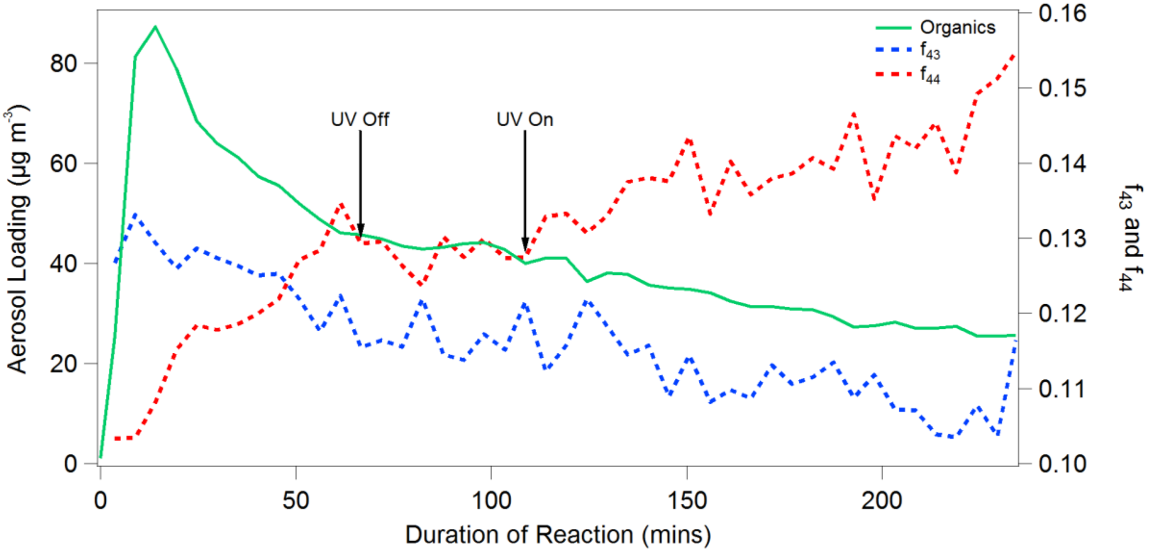

Figure S1: Five-minute averages of loss-corrected SOA concentration, f_{44}, and f_{43} observed for Exp A5. UV lights were turned on and off as labeled. f_{44} and f_{43} could be interpreted as proxies for oxidized and fresh SOA components, respectively, which did not evolve in the dark. Slight SOA loss was observed in the dark, possibly due to loss of organic vapor to the Teflon® wall surfaces. Considering that f_{44} increased and f_{43} decreased as SOA decreased with UV lights on, aging and fragmentation of SOA under UV appear to be driven by photo-oxidation.

S3 CIMS signal normalization: ACIMS vs P-ACIMS

Chemical ionization by hydronium ion in CIMS could be described as

$$\text{Clustering}: H_3O^+\left(H_2O\right)_n + X \xrightarrow{k} XH^+\left(H_2O\right)_n + H_2O$$

$$\text{Protonation}: H_3O^+\left(H_2O\right)_n + X \xrightarrow{k} XH^+ + \left(n+1\right)\left(H_2O\right)$$

where X represents an analyte, and $H_3O^+(H_2O)_n$ represents the hydronium reagent cluster. k is protonation rate coefficient (de Gouw and Warneke, 2007; Sellegri et al., 2005). A reverse of the above process is possible, but could be minimized via instrument tuning (Sellegri et al., 2005). For compound with known proton affinity, the number of water cluster involved in the protonation process, n, is known as well. The proton affinity of isoprene is higher than that of H_3O^+ and lower than that of $(H_3O)^+H_2O$, meaning that n is 0 for isoprene, which could only extract the hydrogen from H_3O^+, forming $C_5H_9^+$, which was observed in our measurements. The charge transfer product ion, $C_5H_8^+$ was also observed. In addition, $C_5H_7^+$, likely a hydride abstraction product by minor reagent ions such as NO^+ or O_2^+, was also observed; fragmentation of oxidized products by $H_3O^+(H_2O)_n$ or minor O_2^+ ions could also produce $C_5H_7^+$ ion fragments, however.

Instrument sensitivity may change over the course of an experiment or between experiments and needs to be accounted for. For simplification, consider a single analyte and hydronium reagent ion. The active Chemical Ionization Mass Spectroscopy (ACIMS) formula could be applied to account for the sensitivity change (de Gouw and Warneke, 2007),

$$\left[XH^+\right] = \left[H_3O^+\right]_0 \left\{1 - \exp\left(-k\tau\left[X\right]\right)\right\} \approx \left[H_3O^+\right] k\tau\left[X\right]$$

where τ is the duration of the protonation process, $[H_3O^+]_0$ is the reference reagent ion signal, [X] is the analyte mass concentration, and $[XH^+]$ is the ion signal. The approximation is valid for very small kτ values (de Gouw and Warneke, 2007). Mathematically, the approximation is valid for exp(-kτ[X]) << 1. Linear signal normalization and species quantification were therefore possible via the following equations,

$$[\mathrm{X}] = \frac{1}{k\tau}\frac{[XH^+]}{[H_3O^+]} = \frac{1}{k\tau[H_3O^+]_0}[H_3O^+]_0\frac{[XH^+]}{[H_3O^+]} = \rho_{cal}\frac{[H_3O^+]_0}{[H_3O^+]}[XH^+] = \rho_{cal}[XH^+]_{norm}$$

$$\rho_{cal} = \frac{1}{k\tau[H_3O^+]_0} \ ; \ k\tau = \frac{[XH^+]_0}{[\mathrm{X}]_0[H_3O^+]_0}$$

$$[XH^+]_{norm} = \frac{[H_3O^+]_0}{[H_3O^+]}[XH^+]$$

where $[XH^+]_{norm}$ is the normalized gas-phase signal and is sufficient for qualitative time-series analysis. In many cases, we do not have standard compounds to obtain a calibration curve and ρ_{cal} remains unknown. The above relations break down when there is significant depletion of reagent ion, where the assumption exp(-kτ[X]) << 1 is no longer accurate, in which case a parallel ACIMS (P-ACIMS) formula should be applied (Wollny, 1998)

$$[X_i] = (k\tau)_i^{-1} \frac{X_iH^+(H_2O)_n}{\sum_j X_jH^+(H_2O)_n} \ln\left[1+\frac{\sum_j X_jH^+(H_2O)_n}{H_3O^+(H_2O)_n}\right]$$

Where $\sum_j X_jH^+(H_2O)_n^+$ is the sum of signals of products from protonation by reagent ion $H_3O^+(H_2O)_n$. For instance, the ratio of quantified concentration by ACIMS to that by P-ACIMS formula is, for n=0 (compounds such as isoprene),

$$[X_i]_{P-ACIMS} = (k\tau)_i^{-1}\frac{[X_iH^+]}{\sum_j[X_jH^+]}\ln\left[1+\frac{\sum_j[X_jH^+]}{[H_3O^+]}\right] = [X_i]_{ACIMS}\frac{[H_3O^+]}{\sum_j[X_jH^+]}\ln\left[1+\frac{\sum_j[X_jH^+]}{[H_3O^+]}\right]$$

$$\frac{[X_i]_{ACIMS}}{[X_i]_{P-ACIMS}} = \left(\frac{[H_3O^+]}{\sum_j[X_jH^+]}\ln\left[1+\frac{\sum_j[X_jH^+]}{[H_3O^+]}\right]\right)^{-1}$$

which is a function of the reagent-to-product signal ratio, $\frac{[H_3O^+]}{\sum_j[X_jH^+]}$, hereafter referred as RPSR, as shown Fig. S2. ACIMS solution overestimates less than 1% compared to P-ACIMS solution for RPSR greater than 500. Overestimation greater than 5 % could be expected for RPSR < 9.8. At RPSR equal to 1, greater than 44 % overestimation could be expected.

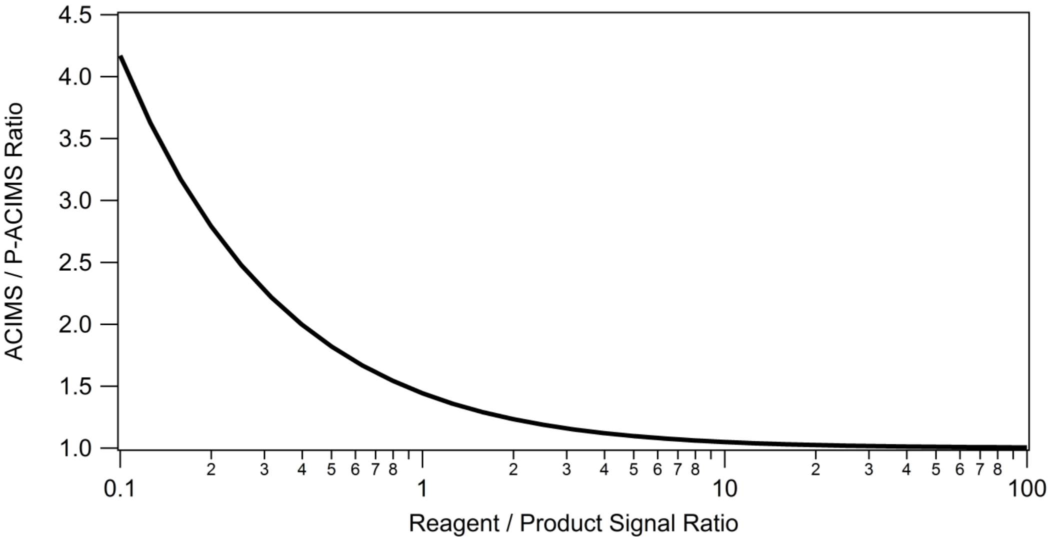

Figure S2: Estimated deviation ratio as a function of reagent-to-product signal ratio (RPSR)

S4 Particulate chloride detection

Low levels of chloride are observed when sampling pure ammonium nitrate, ammonium sulfate, or diacid aerosols, as summarized in Table S1 and illustrated in Fig. S3a. Similar vaporizer effects have been reported for organic artifacts at *m/z* 44 when sampling inorganic salts (Pieber et al., 2016), which is also observed as illustrated in Fig. S3b. The interpretation of chloride mass using the standard fragmentation table, illustrated in Table S2, relies on ions at *m/z* 35 and 36 and expects little interference from other ions. Observed chloride ions when sampling pure ammonium nitrate or ammonium sulfate (Fig. S3a) was likely the result of reactions taking place at the vaporizer surface between sampled species and chlorinated residue.

Table S1: Chloride artifact signal correlations

Species	Slope (μg m^{-3})/(μg m^{-3})	Intercept (μg m^{-3})	R^2
NO_3 (Ammo. Nitrate)	$1.46\ 10^{-2}$	$-2.25\ 10^{-1}$	0.97
SO_4 (Ammo. Sulfate)	$9.66\ 10^{-3}$	$-1.01\ 10^{-2}$	0.80
Organics (Glutaric Acid)	$6.81\ 10^{-3}$	$-4.87\ 10^{-2}$	0.65

[a] Fitting parameter for chloride concentration vs. mass loading of sampled species as shown in Fig. S3a.

Table S2: Treatment of chlorides in standard fragmentation table

m/z	Air[a]	Organic[a]	Chloride[a,b]	Cl[a,b]	HCl[a,b]
28	28				
35			frag_HCl[35],frag_Cl[35]	35, -frag_HCl[35]	0.231*frag_HCl[36]
36	0.00338*frag_air[40]		frag_HCl[36]		36, -frag_air[36]
37		37, -frag_chloride[37]	frag_HCl[37],frag_Cl[37]	0.323*frag_Cl[35]	0.323*frag_HCl[35]
38	0.000633*frag_air[40]	38, -frag_chloride[38], -frag_air[38]	frag_HCl[38]		0.323*frag_HCl[36]
40	0.01458*frag_air[28]				

[a] Species designation used in ACSM

[b] All chloride-related signals at *m/z* 37 and *m/z* 38 are based on *m/z* 35 and *m/z* 36 measurements assuming natural isotopic abundance instead of being directly measured.

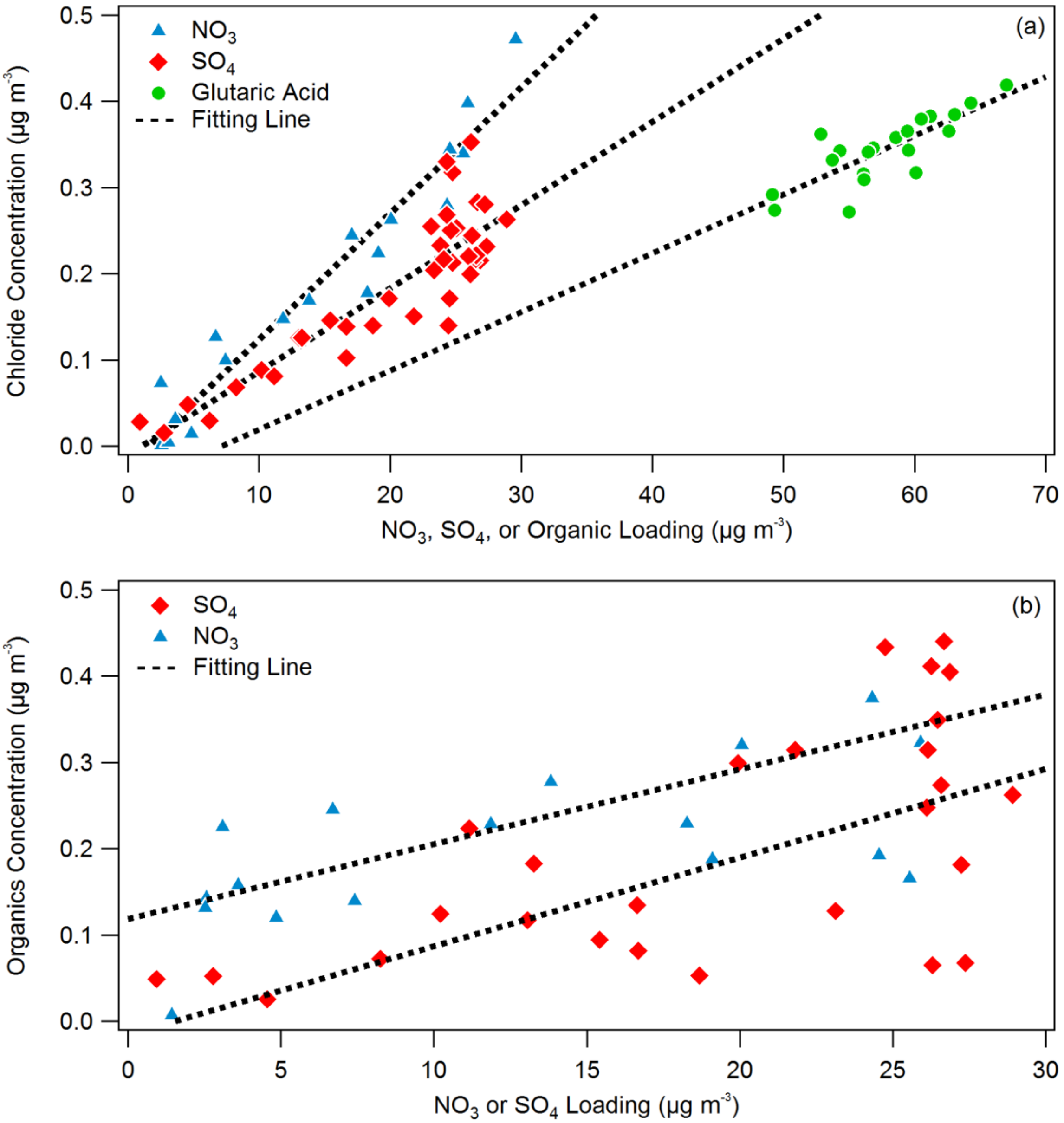

Figure S3: Observation of concentration artifacts for (a) chloride when sampling lab-generated ammonium nitrate, ammonium sulfate, or pure organics aerosols, and for (b) organics when sampling lab-generated ammonium nitrate or ammonium sulfate aerosols

Chloride artifact has been observed by some AMS users as well, though only ammonium nitrate appears to induce noticeable false positive chloride signal (Jose-Luis Jimenez and Weiwei Hu, personal communications). Larger vaporizer effects might be expected in this work considering that the vaporizer effects depend on the vaporizer history (Pieber et al., 2016); additionally, the ACSM used in this work has been exposed to elevated levels of chloride. Figure S4 shows that the reported chloride artifact concentration stems mostly from the HCl^+ (*m/z* 36) ion fragment.

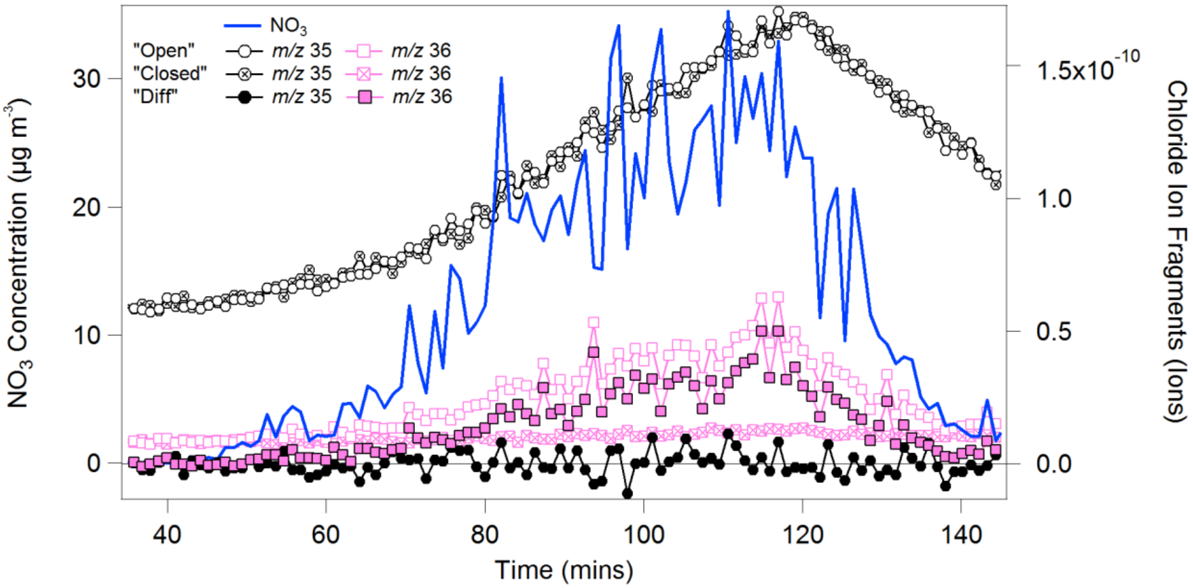

Figure S4: Ion fragments produced at *m/z* 35 and 36 when sampling pure ammonium nitrate. "Diff" stands for "Difference mass spectra"

This does not indicate, however, that only HCl^+ fragments are produced at the vaporizer surface. As seen in Fig. S4, *m/z* 35 "open" and "closed" signals also rise with increasing inorganic non-chloride salt concentrations. The apparent contribution from the *m/z* 35 difference mass spectra is very low because of the elevated background signals. In contrast, background signals at *m/z* 36 are not sensitive towards non-chloride aerosol loading changes. To reduce the vaporizer chloride artifact, long "scrubbing" sessions with inorganic salts may help remove residues from the vaporizer surface.

In the worst scenario, after routine exposure to particulate organic chlorides, the chloride artifact is less than 1.5 % of sampled inorganic nitrate mass (Figure S3a). Because all chamber photooxidation experiments were conducted under low-NO_x conditions using ammonium sulfate as seeding particles, the chloride artifact signal is expected to be well under 1 % of the total aerosol loading. Therefore, vaporizer effects alone cannot explain the high initial chloride loading (9.38 % of total SOA mass) observed in Exp. H1.

A high concentration, initial chlorine injection experiment was carried out (Exp. H2) to further explore the ability of the ACSM to detect organic chloride. The UV lights were turned on for 5 minutes to form SOA and then turned off. The goal was to isolate the effect of gas-phase chemistry from particulate chloride detection. The aerosol sample was continuously passed through an unheated and a heated sampling tube at 1 liter per minute (LPM). As expected, lower OA concentrations were observed when sampling through the heated tube due to aerosol evaporation. Alternate sampling from unheated and heated sampling tubes introduced OA mass step changes, the magnitude of which depended on the temperature set-point. As shown in Fig. S5a, each step change perturbed the vaporizer surface condition, resulting in a concentration “spike” until a new stable condition was achieved, as marked by the signal “rebound”, as illustrated in Fig. S5b.

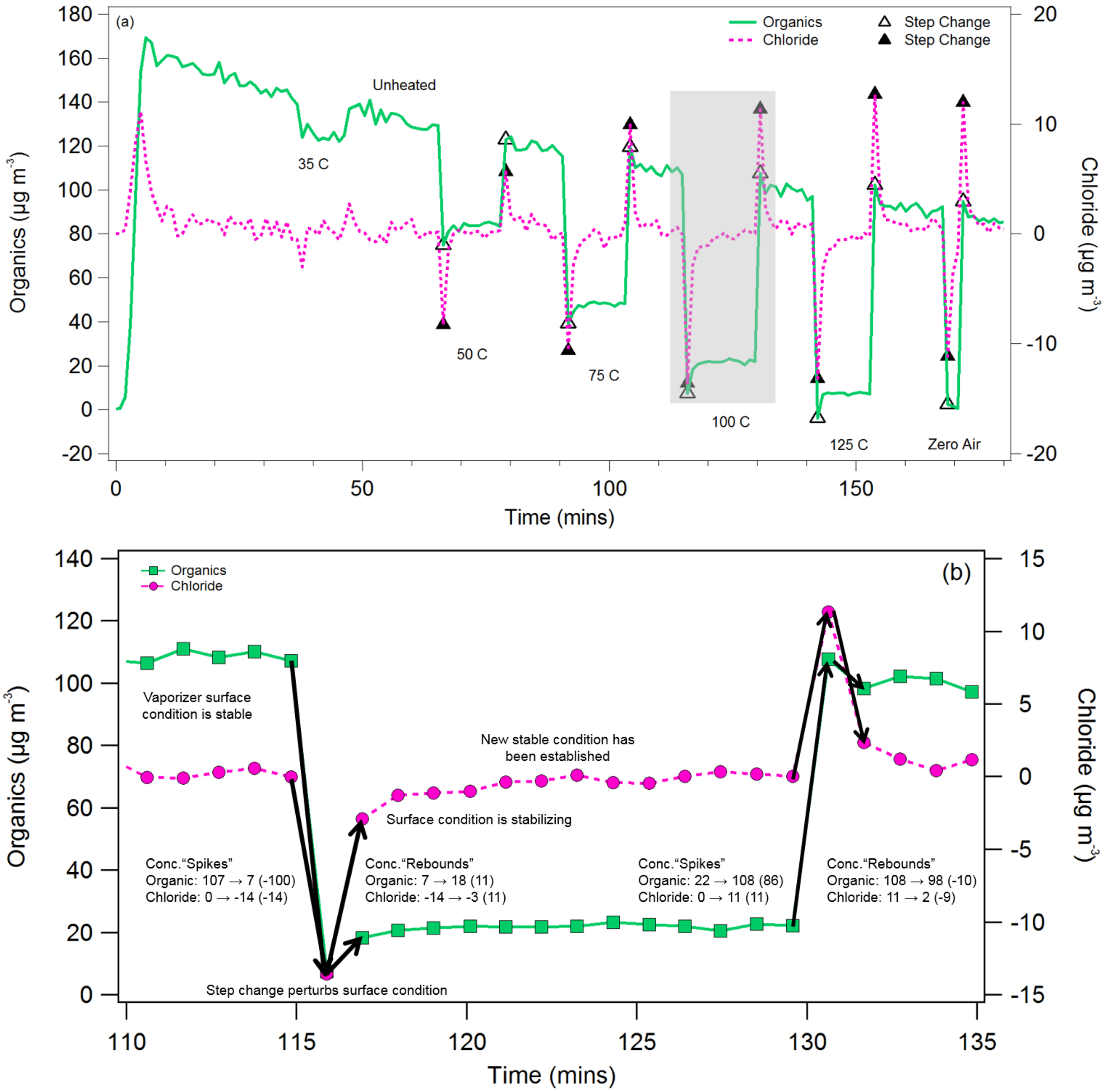

Figure S5: (a) Raw particulate organics and chloride measurement for Exp. H2. Aerosol was alternately passed through heated and unheated sampling lines; annotations show the heated line centerline temperatures. The shaded region is used to illustrate the definition of “spikes” and “rebounds” in (b).

For each step decrease in aerosol concentration, the concentration "spike" (calculated as a concentration change) was negative and the concentration "rebound" (calculated as a concentration change) was positive. For each step increase in aerosol concentration, the concentration "spike" was positive and concentration "rebound" was negative. The correlation between organic and chloride "spike" and "rebound" concentrations is shown in Fig. S6.

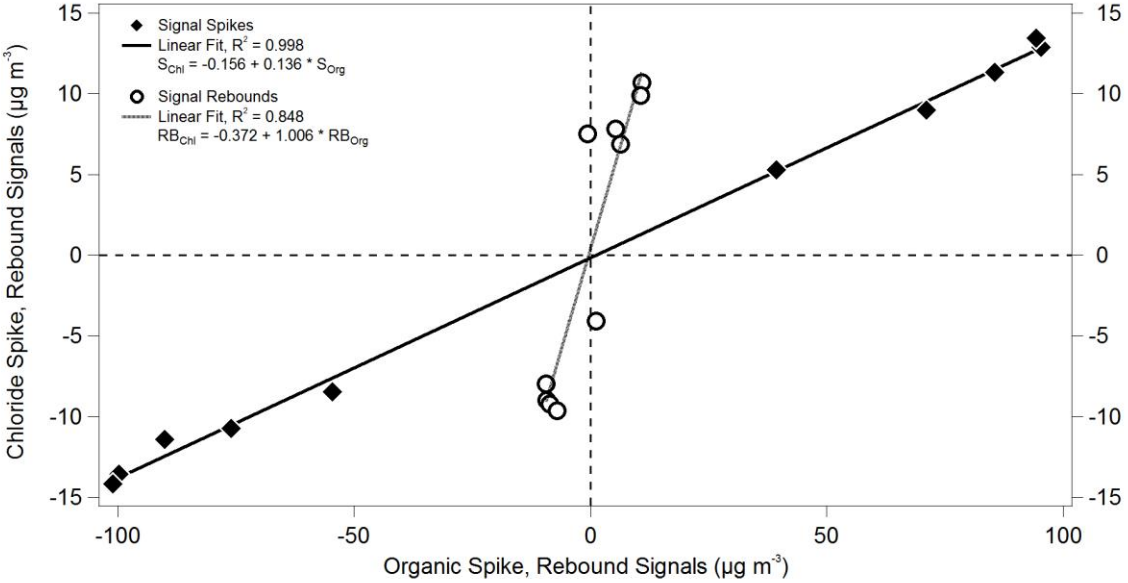

Figure S6: Organics and chloride spikes and rebounds observed following each step change for Exp. H2. Good linear correlation between organics and chloride was observed for both signal spikes ($R^2 \sim 0.998$) and rebounds ($R^2 \sim 0.848$).

The signal "spikes" and "rebound" were likely caused by the slow vaporization of particulate chloride. Two distinct types of chloride ions could be observed in ACSM. As shown in Fig. S7a and S7b, while the fast-desorbing chloride (HCl^+, *m/z* 36) ion fragment correlated well with OA, the slow-desorbing (Cl^+, *m/z* 35) ion fragments anti-correlated with OA, where the background Cl^+ signal was consistently higher than the sample Cl^+ signal. Except for signal "spikes" and "rebounds," the ratio of Cl^+ to HCl^+ was roughly -1:1, which is why the reported chloride concentration was near zero most of the time, even when particulate chlorides might be present. As shown in Fig. S7b, the slow-desorbing chloride (Cl^+, *m/z* 35) was responsible for the observed chloride spikes seen in Fig. S5a. The magnitudes of the chloride and organic spikes are shown in Fig. S6 to correlate very well ($R^2 > 0.998$) over a wide desorption (50–125 °C) and concentration (0–160 $\mu g\ m^{-3}$) range, indicating that particulate organic chlorides were likely present during the experiment, and that they did not differ significantly from other OA components in volatility. Good linear correlation ($R^2 > 0.848$) was also observed for the chloride and organic signal rebounds with a slope of 1, or equal parts Cl and organics ions. The signal rebound was probably due to the build-up/removal of slow-desorbing chloride residues following each step decrease/increase in aerosol concentration. This suggests that the slow-desorbing chloride compounds could have undergone decomposition or oxidation on the vaporizer surface to produce a mixture of compounds such as COCl (55.9% Cl by mass), C_2H_3OCl (45.2% Cl), CO_2Cl (44.6% Cl), etc. resulting in high background chloride signal.

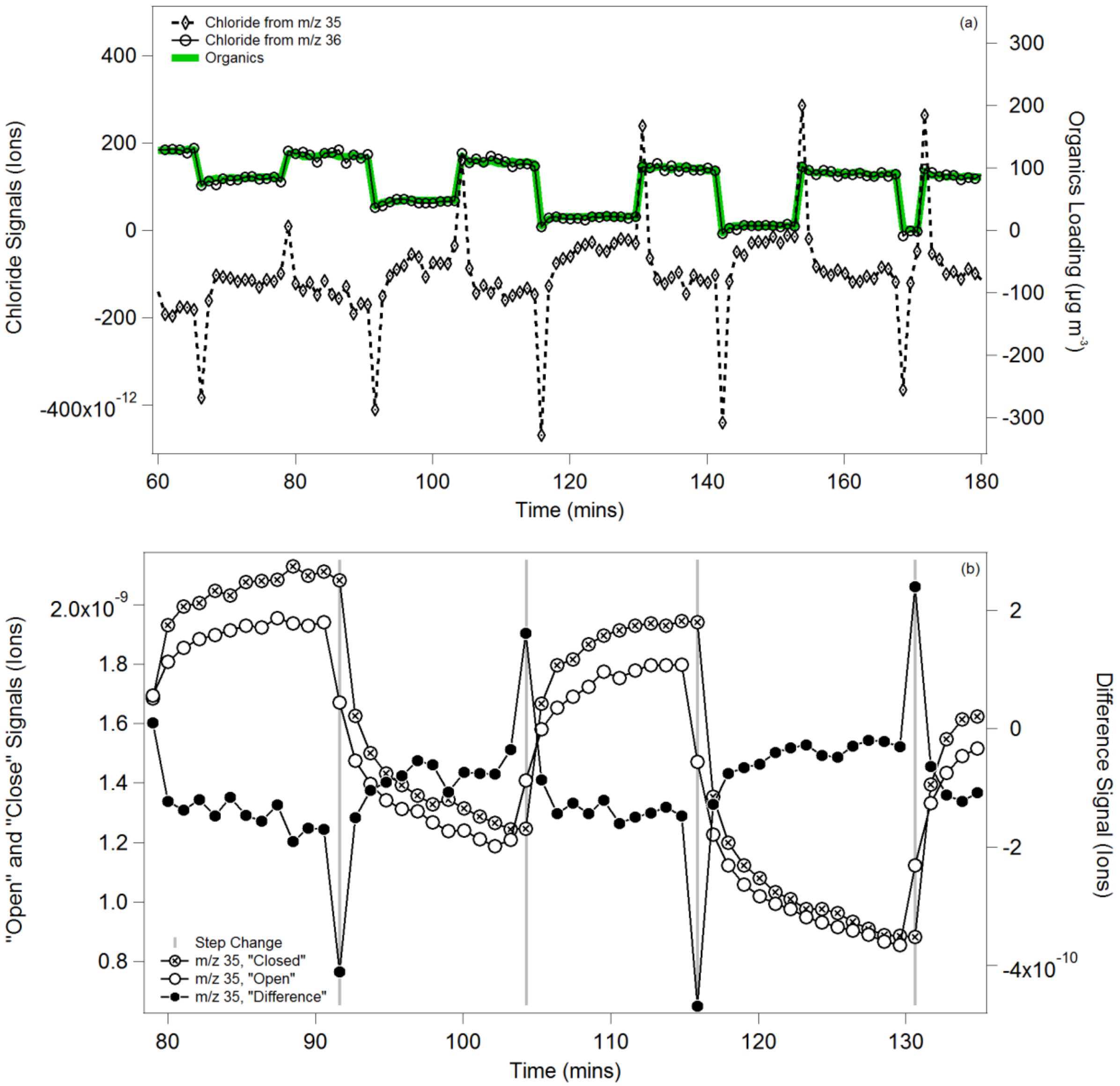

Figure S7: (a) Fast (*m/z* 36)- and slow (*m/z* 35)-desorbing chloride signals measured by the ACSM. Ion fragments at *m/z* 35 and 36 correspond to $^{35}Cl^+$ and $H^{35}Cl^+$ ion fragments. Contribution by $^{37}Cl^+$ and $H^{37}Cl^+$ (not shown) were calculated based on $^{35}Cl^+$ and $H^{35}Cl^+$ assuming natural isotopic abundance. The chloride "spikes" and "rebounds" shown in Fig. S5 are consistent with $^{35}Cl^+$ behavior (b) The slow thermal desorption of chloride species at *m/z* 35 (Cl^+) leads to elevated background chloride signals. To acquire each "difference" mass spectrum used to calculate aerosol loading, the "closed" spectrum is measured first to determine instrument background, after which the "open" spectrum is then measured. Recall that HCl^+ background is much less sensitive towards loading changes, as shown in Fig. S4.

Considering only HCl^+ ion fragments, which correlates well with OA mass, we observe the Cl-to-organics ratio to be around 0.072 ± 0.01. The ratio does not appear to correlate with isoprene concentration, chlorine concentration, or isoprene-to-chlorine ratio, as shown in Fig. S8.

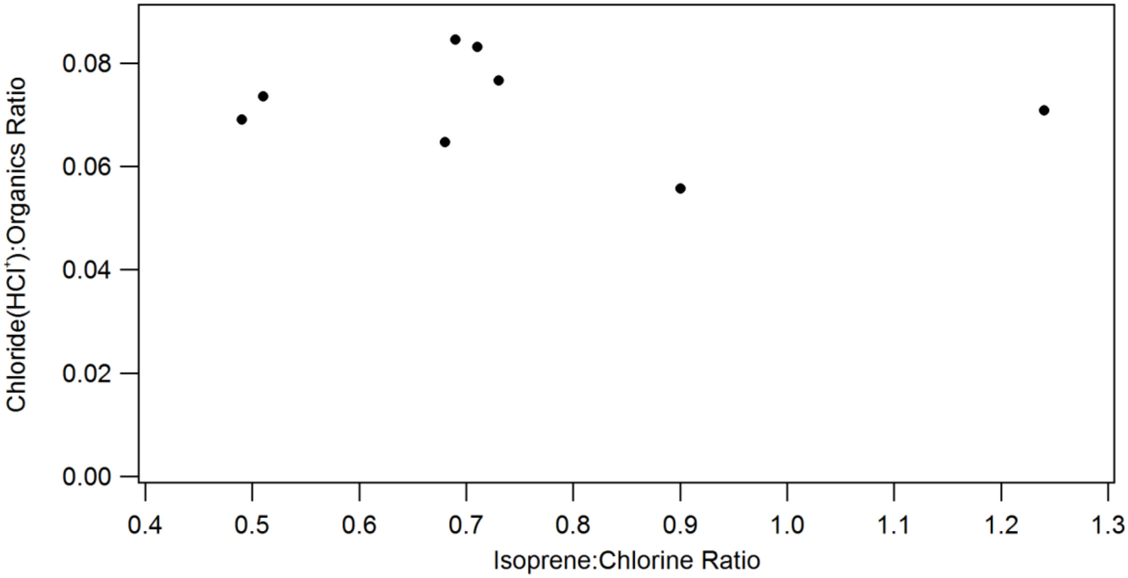

5 **Figure S8:** Averaged particulate chloride-to-organics ratio for Exp. A3–A5, C2–C4, H1, and H2 plotted against precursor isoprene-to-chlorine ratio. Particulate Cl concentration was estimated based on *m/z* 36 ion fragment ($H^{35}Cl^+$) measurement only. Exp A1, A2, and C1 were excluded from analysis due to low chloride mass concentrations. Chloride-to-organics ratio is uncorrelated with isoprene-to-chlorine ratio ($R^2 < 0.05$), isoprene concentration (not shown, $R^2 < 0.22$), or chlorine concentration (not shown, $R^2 < 0.08$).

S5 Effects of data selection on 1-D VBS parameter fitting

Table S3 shows parameters from VBS fits attempting to replicate a yield curve defined by complete VOC consumption where the initial VOC concentration (VOC_0) is 111 µg/m^3, same as the isoprene concentration used in Exp C1. Fitted VBS parameters fail to approximate the linear correlation between Y and VOC_o.

Table S3: Fitted VBS parameters for $Y = C_{OA} / VOC_0$

C*	10^{-4}	10^{-3}	10^{-2}	10^{-1}	10^{0}	10^{1}	10^{2}	10^{3}	10^{4}	10^{5}
10 Bins	0	0	0	0	0	0	1	1	1	1
4 Bins	0	0	0	$3.35\ 10^{-3}$						
		0	0	0	$2.28\ 10^{-2}$					
			0	0	0	$2.08\ 10^{-1}$				
				0	0	$2.09\ 10^{-2}$	1			
					0	0	1	1		
						0	1	1	1	
							1	1	1	1
6 Bins	0	0	0	0	0	$2.08\ 10^{-1}$				
		0	0	0	0	$2.09\ 10^{-2}$	1			
			0	0	0	0	1	1		
				0	0	0	1	1	1	
					0	0	1	1	1	1

[a] VBS fitting was performed in Matlab using the *fmincon* function. VBS parameters (α_i values) are constrained to between 0 and 1.

It is clear that 1-D VBS fitting should not and cannot be applied to yield data collected post VOC depletion. This is further illustrated in Fig. S9 for Exp. C1: VBS fittings were performed on data collected before isoprene depletion ("Pre-depletion") and on the entire dataset ("Full"). By incorporating yield data collected post isoprene depletion, the "Full" yield curve more closely resembles the pre-defined yield curve ($Y = C_{oa} / VOC_0$). Recall that while "pre-depletion" curve should be unique to chlorine-isoprene oxidation, the pre-defined yield curve is not

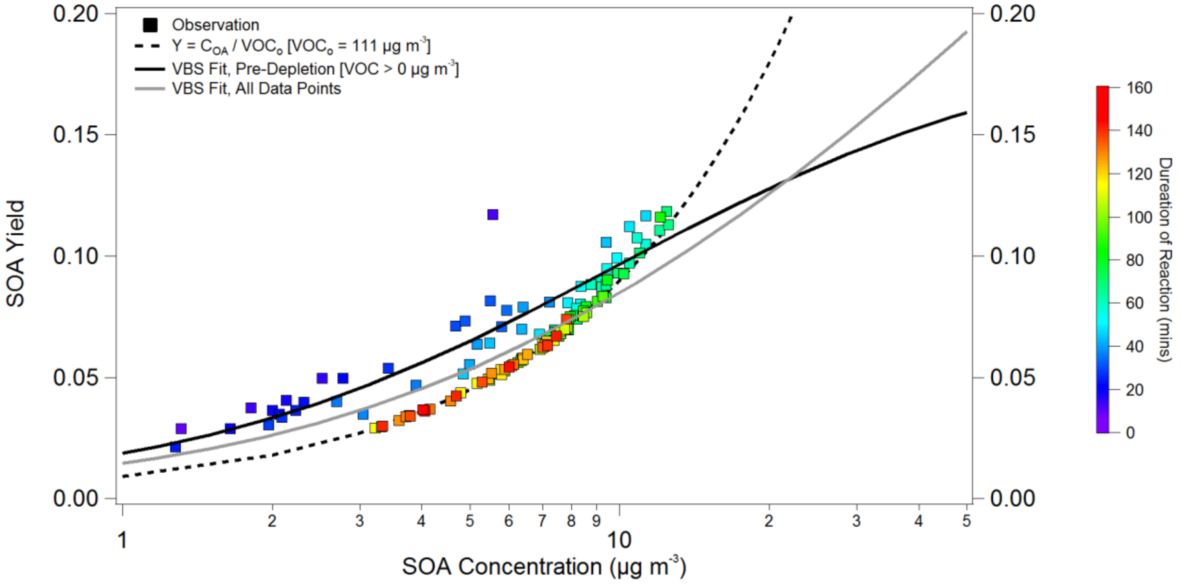

Figure S9: 1-D VBS fitting for Exp C1 with and without incorporating post depletion data.

Table S4 shows the biases introduced to the VBS results, where the "Full" fitting parameters were significantly biased towards higher volatility bins, under-predicting aerosol yield for $C_{OA} < 22$ µg m^{-3} and over-predicting for $C_{OA} > 22$ µg m^{-3}. "Full" case fitting also overestimates the maximum yield, Y_{max}, because the "pre-defined" curve has an unlimited Y_{max}.

Table S4: Comparison of fitted VBS parameter

α_i at C^*_i	0.1	1	10	100	Y_{max}[b]
Pre-Depletion[a]	1.53 10^{-4}	2.63 10^{-3}	1.88 10^{-1}	0	1.91 10^{-1}
Full	7.78 10^{-4}	1.21 10^{-3}	1.13 10^{-1}	2.89 10^{-1}	4.04 10^{-1}

[a] "Pre-Depletion" fitting considers only data acquired prior to the complete consumption of isoprene; "Full" fitting encompasses measurements acquired after isoprene depletion;

[b] Maximum SOA yield, see Eq. (5)

References

Canagaratna, M. R., Jimenez, J. L., Kroll, J. H., Chen, Q., Kessler, S. H., Massoli, P., Hildebrandt Ruiz, L., Fortner, E., Williams, L. R., Wilson, K. R., Surratt, J. D., Donahue, N. M., Jayne, J. T. and Worsnop, D. R.: Elemental ratio measurements of organic compounds using aerosol mass spectrometry: Characterization, improved calibration, and implications, Atmos. Chem. Phys., 15(1), 253–272, doi:10.5194/acp-15-253-2015, 2015.

Donahue, N. M., Kroll, J. H., Pandis, S. N. and Robinson, A. L.: A two-dimensional volatility basis set-Part 2: Diagnostics of organic-aerosol evolution, Atmos. Chem. Phys., 12(2), 615–634, doi:10.5194/acp-12-615-2012, 2012.

de Gouw, J. and Warneke, C.: Measurements of volatile organic compounds in the earth's atmosphere using proton-transfer-reaction mass spectrometry, Mass Spectrom. Rev., 26(2), 223–257, doi:10.1002/mas.20119, 2007.

Heald, C. L., Kroll, J. H., Jimenez, J. L., Docherty, K. S., Decarlo, P. F., Aiken, A. C., Chen, Q., Martin, S. T., Farmer, D. K. and Artaxo, P.: A simplified description of the evolution of organic aerosol composition in the atmosphere, Geophys. Res. Lett., 37(8), doi:10.1029/2010GL042737, 2010.

Kroll, J. H., Donahue, N. M., Jimenez, J. L., Kessler, S. H., Canagaratna, M. R., Wilson, K. R., Altieri, K. E., Mazzoleni, L. R., Wozniak, A. S., Bluhm, H., Mysak, E. R., Smith, J. D., Kolb, C. E. and Worsnop, D. R.: Carbon oxidation state as a metric for describing the chemistry of atmospheric organic aerosol., Nat. Chem., 3(2), 133–139, doi:10.1038/nchem.948, 2011.

Pieber, S. M., El Haddad, I., Slowik, J. G., Canagaratna, M. R., Jayne, J. T., Platt, S. M., Bozzetti, C., Daellenbach, K. R., Fröhlich, R., Vlachou, A., Klein, F., Dommen, J., Miljevic, B., Jiménez, J. L., Worsnop, D. R., Baltensperger, U. and Prévôt, A. S. H.: Inorganic Salt Interference on CO 2 + in Aerodyne AMS and ACSM Organic Aerosol Composition Studies, Environ. Sci. Technol., 50(19), 10494–10503, doi:10.1021/acs.est.6b01035, 2016.

Sellegri, K., Umann, B., Hanke, M. and Arnold, F.: Deployment of a ground-based CIMS apparatus for the detection of organic gases in the boreal forest during the QUEST campaign, Atmos. Chem. Phys., 5(2), 357–372, doi:10.5194/acp-5-357-2005, 2005.

Wollny, A.G.: Flugzeugmessungen atmosphärischer Spurengase mittels Ionen-Molekül-Reaktions-Massenspektrometrie, 1998. Retrieved with permission from University Library Heidelberg BPA. SWB-PPN: 074540750